Journal of Applied Electrochemistry **30**: 1015–1021, 2000.

On modelling molten carbonate fuel-cell cathodes by electrochemical potentials

J.D. FEHRIBACH[1], J.A. PRINS-JANSEN[2], K. HEMMES[2], J.H.W. DE WIT[2] and F.W. CALL[3]
[1]*Department of Mathematical Sciences, Worcester Polytechnic Institute, 100 Institute Road, Worcester, MA 01609-2247, USA*
[2]*Faculty of Applied Sciences, Delft University of Technology, Rotterdamseweg 137, NL-2628 AL Delft, The Netherlands*
[3]*Department of Mechanical and Industrial Engineering, Marquette University, PO Box 1881, Milwaukee, WI 53201-1881, USA*

Received 24 October 1999; accepted in revised form 21 March 2000

Key words: electrochemical potentials, modelling, molten carbonate porous electrodes

Abstract

We derive an electrochemical-potential model for the peroxide mechanism describing the electrochemistry of a molten carbonate fuel cell cathode. The advantages of this model include elegantly combining the chemical and electrical processes, making clear the connection to the underlying reaction stoichiometry, and requiring the fewest equations consistent with that stoichiometry. The relationship between electrochemical-potential and concentration models is also discussed, along with a two-dimensional computational study of the effects of variations in electrode geometry or coefficient parameters. In particular, it is shown that the mean current density associated with a small portion of electrode may be increased by as much as a factor of five by carefully redistributing the electrolyte, and that on this scale the current density is most sensitive to the electrolyte diffusivity.

List of symbols

c_X	concentration of species X (mol cm^{-3})
c_X^{eq}	equilibrium concentration of species X (mol cm^{-3})
D_X	diffusion coefficient of species X (cm^2 s^{-1})
F	faradaic constant (96 500 C mol^{-1})
i_0	exchange current density (mA cm^{-2})
i_0^0	standard exchange current density (mA cm^{-2})
i_F	faradaic current density (mA cm^{-2})
$\boldsymbol{n}$	norm vector at interface $\partial\Omega_{ab}$ (points from a towards b)
p_X	partial pressure of species X at 1 atm
R	gas constant (8.314 J (mol K)$^{-1}$)
t	time (s)
T	temperature (K)
x, y	position (μm)

Greek symbols

α_a, α_c	anodic and cathodic transfer coefficients
β_{es}	inverse reaction resistance (Ω^{-1} cm^{-2})
η_s	surface overpotential (mV)
κ_{ox}, κ_c	component electrochemical conductivities (Ω^{-1} cm^{-1})
ϕ_e, ϕ_s	electrolyte, solid-electrode electrical potential (mV)
ϕ_e^{eq}, ϕ_s^{eq}	equilibrium electrolyte, solid–electrode electrical potential (mV)
μ_X	electrochemical potential of species X (J mol^{-1})
μ_X^{eq}	equilibrium electrochemical potential of species X (J mol^{-1})
μ_{ox}, μ_c	component potentials (J mol^{-1})
σ	electrolyte conductivity (Ω^{-1} cm^{-1})
$\Omega_g, \Omega_e, \Omega_s$	gas, electrolyte and solid phases within the computational electrode
$\partial\Omega_{ab}$	phase boundary (between phase a and phase b)

1. Introduction

This paper presents a steady-state, electrochemical-potential model for a molten carbonate fuel-cell (MCFC) cathode, then applies the model in a computational study of the effects of variations in either electrode geometry or the values of reaction and diffusion parameters on a small portion of cathode. In this model, the electrochemical potentials for individual species are combined to define *component potentials* which are 'separated' by the slow chemical and/or electrochemical reactions. The reaction rates for the slow reactions are assumed to be proportional to the differences in these component potentials, hence we are assuming linear kinetics. This is the classical view of nonequilibrium thermodynamics of, say, Onsager (cf. e.g. [1], pp. 5*ff*) applied to fuel cell electrodes; it is valid on the scale of these computations, and it simplifies our

work by reducing the number of unknowns to be determined. This simplification aids in a study of MCFC cathodes that would be difficult or impossible to reproduce experimentally because of the smallness of the scale. In all, this model takes into account the reactions, diffusion and conduction in the cathode.

The paper is divided into two main parts. The first part is a brief derivation of an electrochemical-potential model for one version of the peroxide mechanism. This version was used by Prins et al. [10] in the development of the three-phase homogeneous model for MCFC electrodes. The derivation discusses the connection between electrochemical potentials and the concentration model by tying the latter to its underlying stoichiometry. The second part examines cathode performance, first by considering the mean current density produced by a computational cross section designed to approximate the cross section shown in Figure 1, then by determining how this current density changes when either a specific parameter value or the geometry is changed. The effects of parameters on performance have been previously studied (e.g. [4]), but earlier studies have not specifically tried to reproduce physical electrode cross sections such as Figure 1. Our study suggests that appropriately redistributing the electrolyte in the cathode can more than quadruple the mean current density, and that on the length-scale of this study, the electrolyte diffusivity is the most important single parameter of those considered in determining cathode performance.

2. A peroxide mechanism model

In the peroxide mechanism, the cathode reaction ($O_2 + 2\,CO_2 + 4\,e^- \rightleftharpoons 2\,CO_3^{2-}$) is achieved through a sequence of steps shown schematically in Figure 2. Each of the reaction steps occurs at one of the four dots in the diagram, and the arrows in the diagram give the forward direction for the mechanism. The location of each reaction follows the description of the mechanism given by Yuh and Selman [16], except for the reaction that produces peroxide ions which we assume occurs at the electrolyte–solid interface. This assumption is analogous to that of Makkus, Hemmes and de Wit [7] for the superoxide mechanism.

When the entire mechanism is at equilibrium (i.e., when the forward arrows in Figure 2 are exactly balanced by backward arrows in the opposite direction), one can write a sequence of equalities for electrochemical potentials, moving from the oxidant side of Figure 2 across the diagram to the current side:

$$\begin{aligned}\mu_{O_2} + 2\mu_{CO_2} &= 2\mu_{O_2^{2-}} - 2\mu_{CO_3^{2-}} + 4\mu_{CO_2}\\ &= 2\mu_{O_2^{2-}} + 2\mu_{CO_3^{2-}} - 4\mu_{O^{2-}}\\ \hline &= -2\mu_{e^-} - 2\mu_{O^{2-}} + 2\mu_{O^-} + 2\mu_{CO_3^{2-}}\\ &= -4\mu_{e^-} + 2\mu_{CO_3^{2-}}\end{aligned} \qquad (1)$$

The dividing line in the above expression indicates that the reaction that consumes peroxide is assumed rate-determining. Based on this division, one can define the following *component potentials*:

$$\left.\begin{aligned}\mu_{ox} &:= \mu_{O_2} + 2\mu_{CO_2}\\ \mu_c &:= -4\mu_{e^-} + 2\mu_{CO_3^{2-}}\end{aligned}\right\} \qquad (2)$$

The separation of the oxidant (ox) and current (c) component potentials is depicted schematically by the dashed line in Figure 2. When the entire mechanism is at equilibrium, $\mu_{ox} = \mu_c$.

When the entire mechanism is *not* at equilibrium, these potentials differ because of the rate-determining reaction separating them, and a system of differential equations is needed to describe how the mechanism proceeds. Let Ω_g, Ω_e and Ω_s be, respectively, the gas, electrolyte and solid phases of this volume, and let $\partial\Omega_{ge}$, $\partial\Omega_{es}$ and $\partial\Omega_{sg}$ be the interfaces between these phases. Since the electrons and carbonate ions are present in excess in their respective phases, the chemical potentials for these species are uniformly constant at their equilibrium values. Therefore, it is useful to split μ_c into its solid and electrolyte portions ($\mu_c =: \mu_{cs} + \mu_{ce}$) and then to split each of these portions into their chemical and electrical parts:

$$\left.\begin{aligned}\mu_{cs} &= -4\mu_{e^-} = -4\mu_{e^-}^{eq} + 4F\phi_s \quad \text{in } \Omega_s\\ \mu_{ce} &= 2\mu_{CO_3^{2-}} = 2\mu_{CO_3^{2-}}^{eq} - 4F\phi_e \quad \text{in } \Omega_e\end{aligned}\right\} \qquad (3)$$

where $\mu_{e^-}^{eq}$ and $\mu_{CO_3^{2-}}^{eq}$ are (constant) equilibrium potentials, and ϕ_s and ϕ_e are the electrical potentials in their respective phases. Finally assume that the solid electrode is a perfect conductor with uniform boundary conditions; this assumption (and the fact that potentials are only defined up to an additive constant) allows one to set $\phi_s \equiv \phi_s^{eq} = 0$. Hence, μ_{cs} is constant in Ω_s, and $\nabla\mu_{ce} = -4F\nabla\phi_e$ in Ω_e. For a steady-state cathode where current production is governed by oxidant diffusion, current conduction and the single rate-determining reaction step discussed above, current production is described classically in terms of nonequilibrium thermodynamics by the following linear system of equations:

$$\begin{aligned}&\text{(a) } \nabla\cdot(\kappa_{ox}\nabla\mu_{ox}) = 0 \quad (\text{in } \Omega_g \cup \Omega_e)\\ &\text{(b) } \nabla\cdot\nabla\phi_e = 0 \quad (\text{in } \Omega_e)\\ &\text{(c) } \phi_s = 0 \quad (\text{in } \Omega_s)\\ &\text{(d) } \nabla\phi_e\cdot\boldsymbol{n} = 0 \quad (\text{on } \partial\Omega_{ge})\\ &\text{(e) } \nabla\mu_{ox}\cdot\boldsymbol{n} = 0 \quad (\text{on } \partial\Omega_{sg})\\ &\text{(f) } \kappa_{ox}\nabla\mu_{ox}\cdot\boldsymbol{n} = 4F\kappa_c\nabla\phi_e\cdot\boldsymbol{n}\\ &\qquad\qquad = \beta_{es}(\mu_c - \mu_{ox}) \quad (\text{on } \partial\Omega_{es})\end{aligned} \qquad (4)$$

In the above expressions all of the normal derivatives are one-sided; the direction of $\boldsymbol{n}$ on any interface $\partial\Omega_{ab}$ is from phase *a* into phase *b*, that is, from the first phase in

the boundary subscript, towards the second. The parameters β_{es}, κ_c and κ_{ox} are, respectively, the inverse reaction resistance for the rate-determining reaction step, and the electrochemical conductivities for the current and the oxidant. The inverse reaction resistance is given found by linearizing the Butler–Volmer equation (cf. e.g. [8], p. 187*ff*):

$$i_F = i_0\left[\exp\left(\frac{\alpha_a F}{RT}\eta_s\right) - \exp\left(-\frac{\alpha_c F}{RT}\eta_s\right)\right] \tag{5}$$

where $\eta_s = (\mu_c - \mu_{ox})/F$ is the surface overpotential, and i_F is the faradaic current. Assuming that $|\mu_c - \mu_{ox}|/RT \ll 1$ (which will be the case in the computations below), the right-hand term in Equation (4f) is approximately equal to $i_F F$, provided that $\beta_{es} := i_0(\alpha_a + \alpha_c)F/RT$. The electrochemical conductivity for the current comes from the standard definition of electrical conductivity, σ, and that the central term in Equation 4(f) must also equal $i_F F$. The relationship is simply $\kappa_c = \sigma/4$.

The electrochemical conductivity for the oxidant is proportional to the diffusivities (cf. Landau and Lifschitz [6], pp. 231–232. or Robinson and Stokes [13], p. 287). Here the relationships are

$$\left.\begin{aligned}\kappa_{ox}\frac{\partial\mu_{O_2}}{\partial c_{O_2}} &= \frac{4F^2}{5}D_{O_2}\\ \kappa_{ox}\frac{\partial\mu_{CO_2}}{\partial c_{CO_2}} &= \frac{4F^2}{5}D_{CO_2}\end{aligned}\right\} \tag{6}$$

These relations follow since the temperature and pressure are assumed to be approximately constant inside the cathode. The normalizing coefficients (4/5) in front of the diffusivities are combinations of the stoichiometric coefficients and valences. Combining the above derivations, one sees that the first term in Equation 4(f) also equals $i_F F$:

$$\begin{aligned}\kappa_{ox}\nabla\mu_{ox}\cdot\boldsymbol{n} &= \kappa_{ox}\frac{\partial\mu_{O_2}}{\partial c_{O_2}}\nabla c_{O_2}\cdot\boldsymbol{n} + 2\kappa_{ox}\frac{\partial\mu_{CO_2}}{\partial c_{CO_2}}\nabla c_{CO_2}\cdot\boldsymbol{n}\\ &= F^2\left(\frac{4}{5}D_{O_2}\nabla c_{O_2} + \frac{8}{5}D_{CO_2}\nabla c_{CO_2}\right)\cdot\boldsymbol{n}\\ &= \frac{1}{5}i_F F + \frac{4}{5}i_F F = i_F F\end{aligned} \tag{7}$$

where $D_{O_2}\nabla c_{O_2}\cdot\boldsymbol{n} = i_F/4F$ and $D_{CO_2}\nabla c_{CO_2}\cdot\boldsymbol{n} = i_F/2F$ as in Prins et al. [10].

3. Current density computations

This Section presents a comparison of the mean current densities for three electrode geometries, and considers how adjusting certain of the parameter values affects these mean current densities. The computations presented here are two-dimensional, but all three phases of the cathode (gas, electrolyte and solid) are taken into account. Hence these computations are far more realistic than those of our work on internal resistance for flooded electrodes [2]. The computations are carried out using the PDE Toolbox of Matlab, version 5.1, and are similar to computations presented in [3]. The principal results of this study are (i) that the redistribution of electrolyte in an MCFC cathode can lead to a substantial increase in mean current density (for the geometries considered here, the increase is a factor of 5), and (ii) that knowing the precise values of the exchange current and the electrolyte diffusivity is more important than knowing the precise value of either the gas diffusivity or the electrolyte conductivity in determining the mean current density for a $100 \times 100\,\mu m^2$ cathode cross section.

For the computations presented here, the temperature is set to 923 K, and the electrical potential drop between the solid cathode and the outer edge of the electrolyte (at $x = \pm 50$ or $y = \pm 50$ in Figure 3) is set to 70 mV. From Equation 3, the corresponding drop in electrochemical potential is $4F(0.07\text{ V}) = 27\,020\text{ J mol}^{-1}$. Since the peroxide mechanism is being considered, the anodic and cathodic transfer coefficients are, respectively, $\alpha_a = 1.5$ and $\alpha_a = 0.5$ ([11], p. 3588). The exchange current density is given by

$$i_0 = i_0^0(p_{O_2})^{0.375}(p_{CO_2})^{-1.25} \tag{8}$$

i_0^0 being the standard exchange current density, and p_X being the partial pressure of species X at 1 atm (cf., e.g. [16], p. 2064). As starting values for the computations discussed below, assume that the bulk gas concentration is 50% O_2, 10% CO_2 and that $i_0^0 = 4\text{ mA cm}^{-2}$ ([12], p. 3610). So the exchange current density is then 55 mA cm^{-2}, and hence $\beta_{es} = 1.38(\Omega\,\text{cm}^2)^{-1}$. The oxidant electrochemical conductivity κ_{ox} is found using Equation 6, approximating the partial derivatives using the standard formula for the ideal gas relationship $\mu_X = \mu_X^{eq} + RT\ln(c_X/c_X^{eq})$ and assuming gas diffusivities of $10^{-1}\,\text{cm}^2\,\text{s}^{-1}$ and electrolyte diffusivities of $10^{-5}\,\text{cm}^2\,\text{s}^{-1}$. This is only a lowest-order approximation, but it is a good starting point. Using these values, one finds $\kappa_{ox} = 0.97\,(\Omega\,\text{cm})^{-1}$ in Ω_g, but $\kappa_{ox} = 7 \times 10^{-6}\,(\Omega\,\text{cm})^{-1}$ in Ω_e. Finally since $\sigma = 1.40\,(\Omega\,\text{cm})^{-1}$, $\kappa_c = \sigma/4 = 0.35\,(\Omega\,\text{cm})^{-1}$.

The initial computational domain (cf. Figure 3)* is set up to match as much as possible on the given scale the physical cross section shown in Figure 1. Because of the scaling limitations in defining a computational grid, the match is far from perfect, but please note the similarities, for example, in the gas phases in the lower corners and in the solid phase slightly to the left of the center of the cross section.

Since the bulk gas is in equilibrium with the O_2 and CO_2 concentrations at the electrolyte–solid interface when i_F and η_s are both zero, the outer boundary condition on the computational domain for the oxidant

* Full colour versions of each of the plots presented here can be viewed at http://www.wpi.edu/~bach/ECPplots.

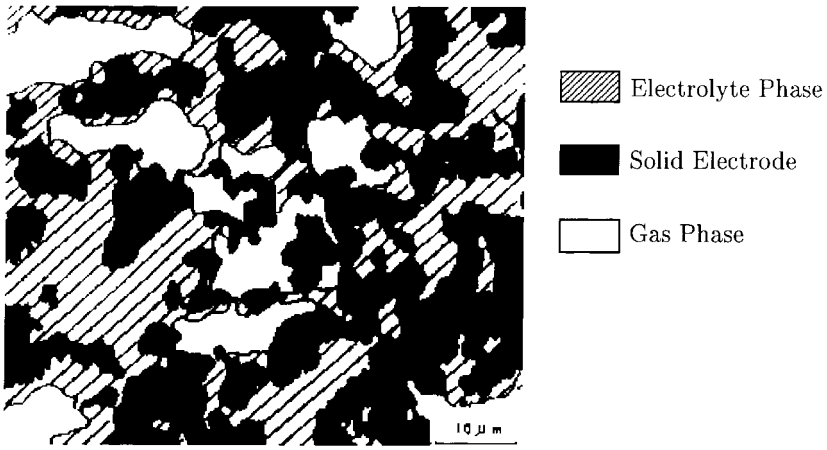

Fig. 1. Physical electrode cross section. Black-and-white depiction of a colour electron probe microanalysis (EPMA) photograph [15]. Similar cross sections are discussed in [5]. Approximate dimensions: 70 μm $\times$ 60 μm.

potential must be $\mu_{ox} = 0$. This condition is applied at the outer edge of the gas phase of the computational domain and along $\partial\Omega_{sg}$. So on $\partial\Omega_{sg}$, the boundary condition used is different from Equation 4(e), but the revised boundary condition allows each portion of the gas phase to be continuously supplied with oxidant gas, and it simulates gas flow into Ω_g from the third dimension (perpendicular to the page). In effect, it allows one to make pseudo three-dimensional computations. The interface conditions for the gas–electrolyte interface and electrolyte–solid interface are all as shown in Equation 4(d), (f). The outer boundary conditions for the electrolyte allow carbonate ions to flow out along each outer edge of Ω_e.

For the parameter values and computational domain described above, Matlab can be used to compute the current density throughout this entire computational cathode. Although the current density is as high as 640 mA cm^{-2} at various interior 'hot-spots', the mean current density along the outer edge of this computational cathode is only 4.9 mA cm^{-2}. This value may seem low compared to a typical standard operating value for MCFC cathodes of roughly 150 mA cm^{-2}, but it is less surprising when one considers how thin this computational cathode is (effectively less than 50 μm), the high fill-percentage and relatively poor electrolyte distribution, and the two-dimensional nature of the calculations. In any event, the precise magnitude of the mean current density for this computational cathode is less important since it is mainly used a reference value to study the performance sensitivity of our small cross section to variations in parameter values and geometry.

First, using the same electrode geometry as before, let us consider what changes occur if we vary, one at a time, the gas diffusivities, the electrolyte diffusivities, the electrolyte electrical conductivity, and the standard

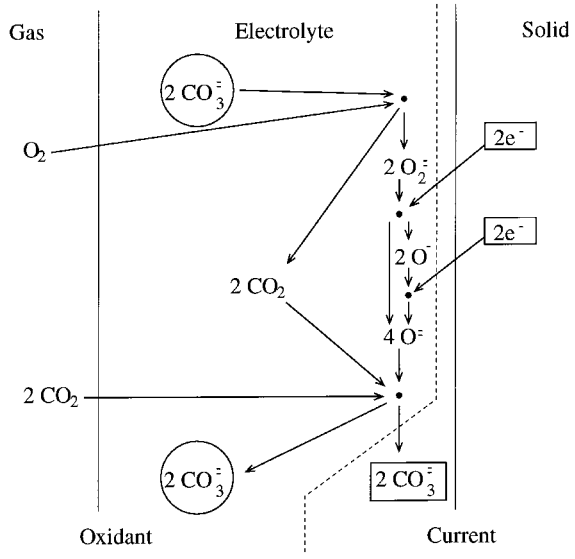

Fig. 2. One net cycle for the peroxide mechanism. Reactions occur at dots, arrows show the forward direction for reactions, solid lines separate phases, dashed lines separate components, current-carriers are in boxes, and carbonate ions which continue from one cycle to the next are circled.

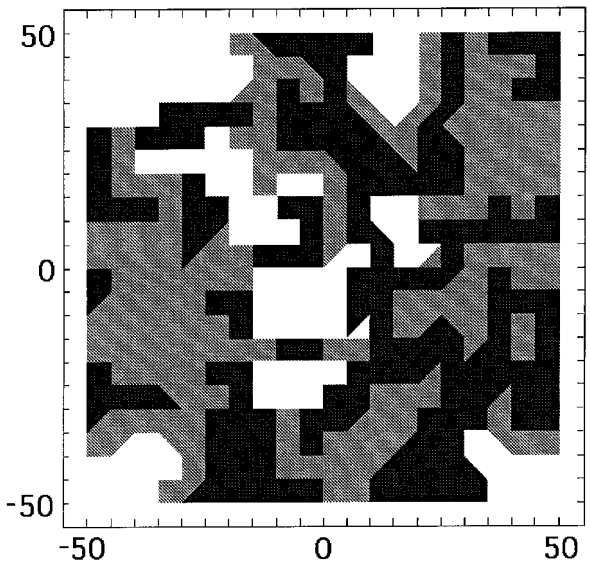

Fig. 3. Initial computational cathode. Gas phase is white; the Electrolyte, grey; the solid, black. Dimensions: 100 μm $\times$ 100 μm.

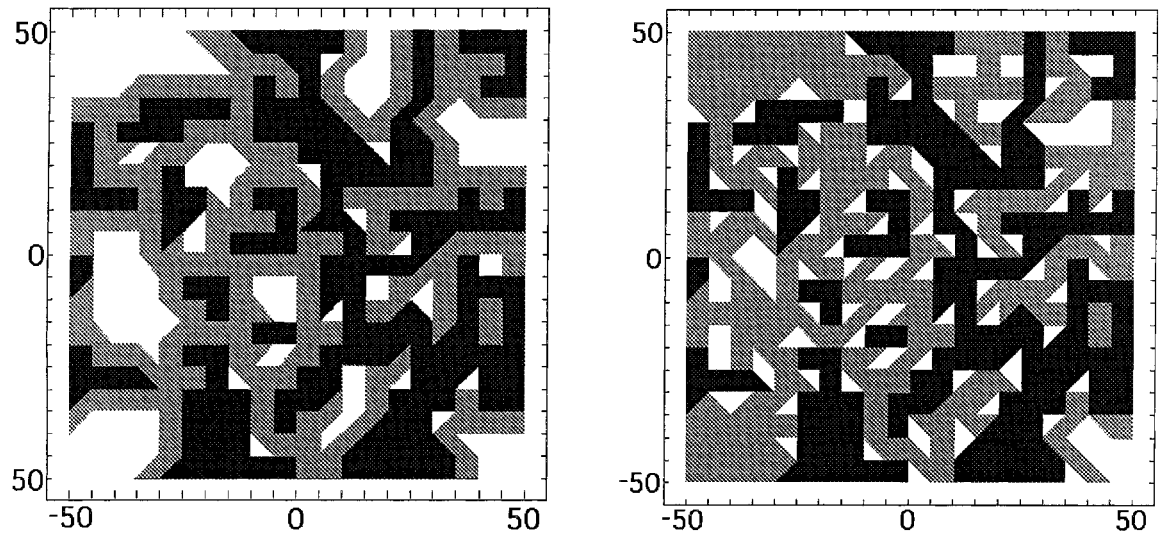

Fig. 4. Two improved computational cathodes. Dimensions: 100 μm $\times$ 100 μm.

exchange current. Computations show that increasing or decreasing either the gas diffusivities or the electrolyte electrical conductivity by a factor of 10 has little or no effect on the current density. This is not surprising considering the relatively large values of the electrochemical conductivities associated with these parameters. Increasing either the electrolyte diffusivity or the standard exchange current, on the other hand, does have a measurable effect. Computations show that increasing the electrolyte diffusivity by a factor of 2 will roughly double the current density (see Table 1), while increasing or decreasing the standard exchange current by a factor of 2 will increase or decrease the mean current density by approximately 10% (see Table 2). Both of these parametric changes are within a physically reasonable range (e.g., Uchida et al. have reported values for the standard exchange current density of 10 mA cm^{-2} [14]).

Next let us consider two 'improved' computational cathodes, that is, ones whose electrolyte has been judiciously redistributed. Two such cathodes are shown in Figure 4. The gas channels in the lefthand cathode are more evenly distributed than in the initial cathode, but the electrolyte still tends to coat the solid electrode; those in the righthand cathode are smaller, still more evenly distributed, and now tend to lie between the solid and the electrolyte. Note that the solid phase has not changed[†]; only the electrolyte and gas have been redistributed. The boundary conditions and parameter values are the same as for the initial case. Because of the improved electrolyte distribution, the current density for each of these improved cathodes reaches maximum levels over 1000 mA cm^{-2} at 'hot-spots', and these more active regions are more widely distributed around the electrode. The moderate redistribution of electrolyte for the left-hand cathode in Figure 4 yields a mean current density across the outer edge of 10 mA cm^{-2}, more than double that of the initial cathode. For the right-hand cathode with its smaller gas channels, the mean current density across the outer edge is 24 mA cm^{-2}, almost five times what it was in the initial case.

Finally, turning our attention to a technical point, recall that in Section 2 above it was shown that the accuracy of these computations hinges on the potential jump at the electrolyte–solid interface $\partial\Omega_{es}$ being sufficiently small, that is, one must require that $|\mu_{ox} - \mu_c|/RT \ll 1$. By directly examining this potential difference, one sees that this condition is easily satisfied for these computations. Indeed on $\partial\Omega_{es}$ for each cross section, one finds that $|\mu_{ox} - \mu_c|/RT < 250/7674 \approx 0.033$.

4. Discussion

This paper has presented an electrochemical formulation of one version of the peroxide mechanism and

Table 1.

Electrolyte diffusivity/cm^2 s^{-1}	Mean current density/mA cm^{-2}
0.5×10^{-5}	2.7
1.0×10^{-5}	4.9
2.0×10^{-5}	8.8

Table 2.

Standard exchange current /mA cm^{-2}	Mean current density /mA cm^{-2}
1.0	3.9
2.0	4.4
4.0	4.9
8.0	5.4

[†] An observant reader will notice that this is not quite true for the left computational cathode near $(x, y) = (0, 5)$ or $(0, 20)$. The computations presented here are at the edge of what Matlab can do. Unfortunately, Matlab cannot create an initial triangulation if the original solid geometry is used for an electrolyte–gas distribution similar to the one on the left in Figure 4.

computations of current densities generated by small portions of simulated MCFC electrodes. One advantage of this approach is that by describing everything (reactions, diffusion and conduction) in terms of potentials, one puts each of these processes on more-or-less the same footing, making comparisons easier. It also reduces the number of equations to be solved and unknowns to be found. Specifically in the computations presented here, we were able to determine current densities *without* having to find the individual concentrations of CO_2 or O_2 in the gas or the electrolyte. Computationally, reducing the number of unknowns to be found both saves time and makes possible the solution of some problems that could not otherwise be solved with presently-available computers and software.

A parameter sensitivity analysis based on our computations indicates that at least on the small scale, the electrolyte diffusivities will be extremely important in optimizing the mean current density for an MCFC cathode. However, the analysis also reveals that the exact value of the exchange current density is less important, and the exact values of the gas diffusivities and the electrolyte conductivity are not important at all. All of this is in keeping with assumptions that are generally made: diffusion limitations can be ignored in the gas phase, but not in the electrolyte phase; the overall reaction rate is limited by transport in the electrolyte rather than being kinetically controlled (e.g., [9]). This is not surprising considering the relative sizes of the electrochemical conductivities. However, it is contrary to the conclusions in our earlier work with the agglomerate and three-phase homogenized models [10–12] where knowing precisely the electrical conductivity was found to be most significant (i.e., rate limiting). This difference may in part be due to the different scales: here we use $100 \times 100\,\mu m^2$ cathode cross section, there we averaged over the entire electrode. Because the current density builds cumulatively as one moves across the thickness of the cathode, mean current density values will be higher if one considers an entire cathode. For a given electrolyte conductivity, these higher values of current density imply a larger voltage drop across the electrolyte, and this in turn would imply that knowing the precise value of the electrolyte conductivity is more important for the entire electrode than it was in our small cross section. Another important contribution to the difference may be the need to use fitting parameters in the early study. The present work has the advantage that there are no such parameters; all parameters used here are directly associated with underlying physical and chemical processes (i.e., diffusion, conduction etc.).

The computations presented here also suggest that the distribution of electrolyte and the physical geometry of the cathode are very important in determining the current density. Relatively flooded portions of cathode with large pockets of electrolyte produce little current, while cathodes with more evenly distributed channels of gas through the electrolyte are much more effective. Again, this statement is not surprising in itself, but using our modeling approach, we are able to find numerical values to show how much improvement can be obtained by effectively redistributing the electrolyte in the cathode. In addition, these computations make clear that distribution is more important than electrolyte fill percentage; the right-hand cathode in Figure 4 has a higher fill percentage than the initial cathode in Figure 3, but the initial one is effectively the more flooded cathode. The importance of the triple points where all three phases meet should also be mentioned; increasing the density of such triple points can greatly increase the current density. However, triple points where the electrolyte forms an acute angled wedge tend to have such high local current densities that they might well tend in degrade in a physical electrode, hurting performance.

Finally, regarding the relatively small size of the current densities computed here, one should keep in mind that these are for a very small portion of a cathode. Since a physical cathode is about ten times thicker (roughly 500–800 μm) than the effective thickness of our computational cathodes, and since current density is cumulative across the thickness of the cathode, one would expect the current densities computed here to be as little as a tenth those measured experimentally for a corresponding physical cathode. Thus, if one were to have a physical cathode made up of many copies of the cross sections considered here, stacked side-by-side and end-to-end, one would expect a mean current density of roughly 50 mA cm^{-2} if the initial distribution were used, and perhaps as much as 100 mA cm^{-2} and 240 mA cm^{-2}, respectively, if the left-hand and right-hand distributions from Figure 4 were used (keeping an overall cathode polarization of 70 mV). As was discussed above, the exact values of the current densities for such cathodes would depend on, among other things, the extent to which finite electrolyte conductivity becomes significant in a laboratory-scale cathode. While a distribution similar to the one in the right-hand cathode in Figure 4, with the gas channels tending to lie between the electrolyte and the solid cathode may be difficult to produce physically, the current density values for the small portions of cathode considered here are quite consistent with the typical measured values of roughly 150 mA cm^{-2} for a 70 mV polarization.

Acknowledgements

J.D.F. was partially supported by the National Science Foundation under the grant DMS-9501022. J.D.F. and K.H. were partially supported by NEDO, the New Energy and Industrial Technology Development Organization of Japan.

References

1. S.R. de Groot, 'Thermodynamics of Irreversible Processes' (North-Holland, Amsterdam, 1951).

2. J.D. Fehribach, J.A. Prins-Jansen, K. Hemmes and J.H.W. de Wit, *in* Proceedings of the Fourth International Symposium on 'Carbonate Fuel Cell Technology' (edited by J.R. Selman, I. Uchida, H. Wendt, D.A. Shores and T.F. Fuller), vol. PV 97-4 (1997), pp. 362–9.
3. J.D. Fehribach, J.A. Prins-Jansen, K.Hemmes and J.H.W. de Wit, *in* Proceedings of the Fifth International Symposium on 'Molten Salt Chemistry and Technology' (1998), pp. 123–6.
4. E. Fontes, M. Fontes and D. Simonsson, *Electrochim. Acta* **41** (1996) 1–13.
5. E. Fontes, C. Lagergren and D. Simonsson, *Electrochim. Acta* **38** (1993) 2669–82.
6. L.D. Landau and E.M. Lifshitz, 'Fluid Mechanics', 2nd edn (Pergamon Press, Oxford, 1987).
7. R.C. Makkus, K. Hemmes and J.H.W. de Wit, *J. Electrochem. Soc.* **141** (1994) 3429–38.
8. J.S. Newman, 'Electrochemical Systems', 2nd edn (Prentice Hall, Englewood Cliffs, NJ, 1991).
9. T. Nishina, I. Uchida and J.R. Selman, *J. Electrochem. Soc.* **141** (1994) 1191–98.
10. J.A. Prins-Jansen, J.D. Fehribach, K. Hemmes and J.H.W. de Wit, *J. Electrochem. Soc.* **143** (1996) 1617–28.
11. J.A. Prins-Jansen, K. Hemmes and J.H.W. de Wit, *Electrochim. Acta* **42** (1997) 3585–600.
12. J.A. Prins-Jansen, K. Hemmes and J.H.W. de Wit, *Electrochim. Acta* **42** (1997) 3601–18.
13. R.A. Robinson and R.H. Stokes, 'Electrolyte Solutions', 2nd edn (Butterworths, London, 1970).
14. I. Uchida, Y. Magikura, T. Nishina and K. Itaga, *J. Electroanal. Chem.* **206** (1986) 229–39.
15. S. Takashima, K. Ohtsuka, N. Kobayashi and H. Fujimura, *in* Proceedings of the Second Symposium on 'Molten Carbonate Fuel Cell Technology' (edited by J.R. Selman, D.A. Shores, H.C. Maru and I. Uchida), vol. PV 90-16 (1990), pp. 378–94.
16. C.Y. Yuh and J. R. Selman, *J. Electrochem. Soc.* **131** (1984) 2062–2069.